Supporting Information belonging to publication

Regioselective *N*- and *C*-Metalation of Neutral 2-Halogenobenzimidazole Derivatives

Rajorshi Das,[†,‡] Jonas Blumberg,[†] Constantin G. Daniliuc,[§] David Schnieders,[§] Johannes Neugebauer,[§] Ying-Feng Han,[‡] and F. Ekkehardt Hahn*[,†,‡]

[†]Institut für Anorganische und Analytische Chemie, Westfälische Wilhelms-Universität Münster, Corrensstrasse 30, D-48149 Münster, Germany

[‡]Key Laboratory of Synthetic and Natural Functional Molecule Chemistry, College of Chemistry and Material Science, Northwest University, Xi'an 710127, P. R. China

[§]Organisch-Chemisches and Center for Multiscale Theory and Computation, Westfälische Wilhelms-Universität Münster, Corrensstrasse 40, D-48149 Münster, Germany

Table of Contents

X-Ray Crystallography

X-ray diffraction data were collected with a Nonius KappaCCD diffractometer equipped with a rotation anode using graphite-monochromated Mo-Kα radiation (λ = 0.71073 Å). Diffraction data were collected over the full sphere and were corrected for absorption. Programs used: data collection: COLLECT,[1] data reduction: Denzo-SMN,[2] absorption correction: Denzo,[3] structure solution: SHELXS-97[4] and structure refinement, SHELXL-97.[5] If not noted otherwise, hydrogen atoms were added to the structure model on calculated positions.

Crystal data for *trans*-[6]. Yellow crystals of complex *trans*-[**6**] were obtained by slow evaporation of the solvent from a tetrahydrofuran solution of the complex at ambient temperature. Formula $C_{19}H_{37}N_4BrNiO_2P_2$, M = 554.08, yellow block, 0.30 x 0.23 x 0.22 mm, a = 8.1734(3), b = 11.9234(5), c = 13.7686(5) Å, α = 87.017(2), β = 75.449(2), γ = 74.890(2)°, V = 1253.78(8) Å^3, ρ_{calc} = 1.468 g·cm^{-3}, μ = 2.516 mm^{-1}, empirical absorption correction ($0.506 \leq T \leq 0.747$), Z = 2, triclinic, space group $P\bar{1}$ (no. 2), λ = 0.71073 Å, T = 173(2) K, ω and φ scans, 100507 intensities collected ($\pm h$, $\pm k$, $\pm l$), ($6.8 \leq 2\theta \leq 67.5°$), 9930 independent ($R_{int}$ = 0.044) and 7865 observed intensities [($I \geq 2\sigma(I)$)], 273 refined parameters, R = 0.0407, wR = 0.0942, R_{all} = 0.0604, wR_{all} = 0.0997, max./min. residual electron density 1.25/–090 e·Å^{-3}. The hydrogen atoms were added to the structure model on calculated positions and were refined as riding atoms.

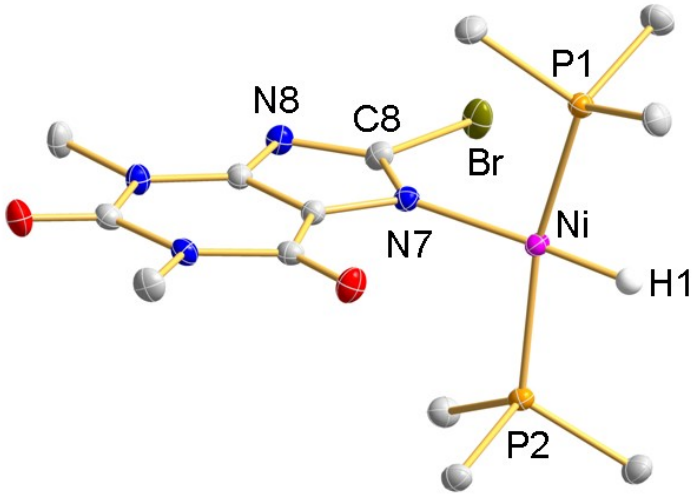

Figure S1. Molecular structures of *trans*-[**6**] (hydrogen atoms except for H1 have been omitted for clarity and only the first atom of the P-ethyl substituents is shown). Selected bond lengths (Å) and angles (deg): Ni–P1 2.1622(6), Ni–P2 2.1684(6), Ni–N7 1.932(2), Ni–H1 1.39(3), N7–C8 1.334(3), N9–C8 1.348(3); P1–Ni–P2 166.86(2), P1–Ni–N7 96.86(6), P1–Ni–H1 85.1(14), P2–Ni–N7 95.81(6), P2–Ni–H1 82.2(14), N7–Ni–H1 177.6(14), N7–C8–N9 118.1(2).

Computational Analysis

All calculations were performed using Turbomole v7.2.1.[6] The PBE0 functional[7] together with the D3 dispersion correction[8] using Becke-Johnson damping[9] was used as it showed very good accuracy in bond activation reactions involving Ni^0 and Pd^0 systems.[10] The def2-TZVP basis set was employed, together with the ECP-60 effective core potentials for Pd.[11] The Turbomole m4 grid was used for numerical integrations. SCF convergence was assumed after energy changes of less than 1E-7 a.u., while geometry convergence thresholds were set to 5E-7 a.u. for energy changes and 1E-3 a.u. for the gradient norm. All optimized structures were confirmed as minima or transition states, respectively, by frequency analyses. Gibbs free enthalpies were calculated using the correction for small vibrational frequencies described in *Chem. Eur. J.* **2012**, *18*, 9955–9964. Solvent effects of THF were included by the COSMO-RS implicit solvent model.[12] Alkyl phosphine ligands PEt_3 were truncated to their methyl analogue, PMe_3.

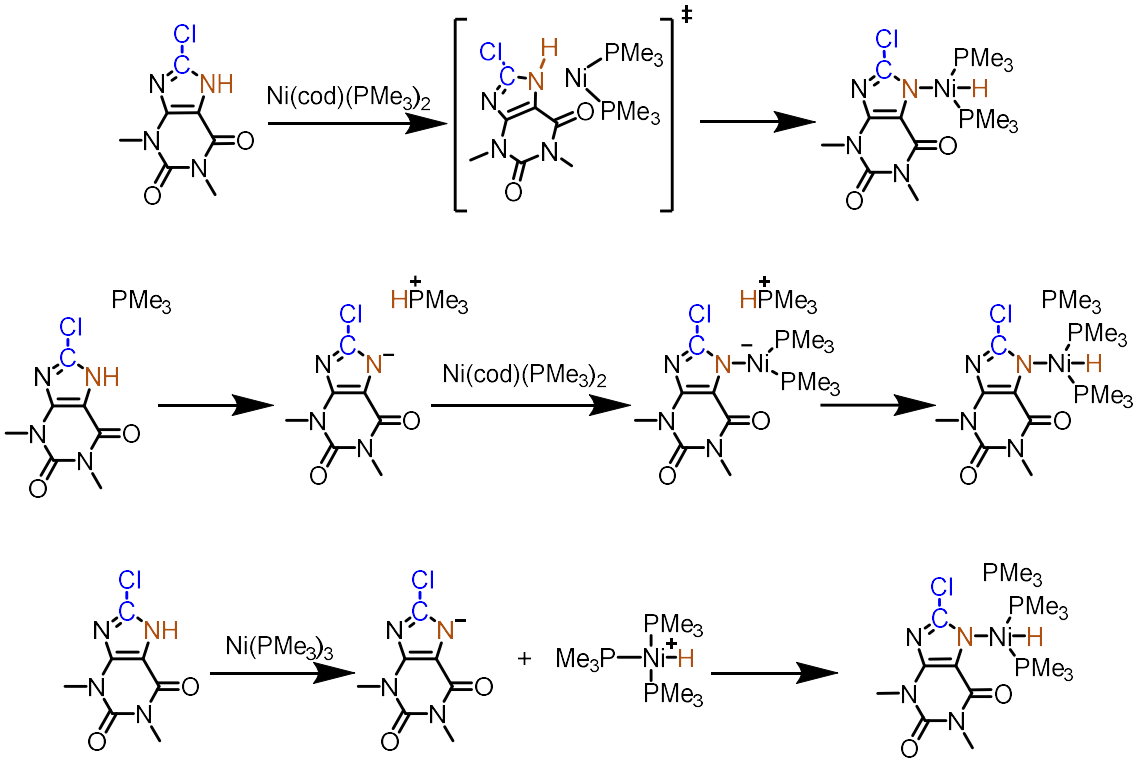

Figure S2. Possible reaction mechanisms leading towards the N-azolato reaction product.

The general mechanism leading to the N-azolato reaction product was determined by an initial study (Figure 2). Three possible reaction mechanisms where considered: a concerted oxidative addition of the N–H bond to the nickel atom (top row), a deprotonation of the N–H group by a phosphine ligand followed by ligation of the nickel atom by the azolato nitrogen atom and protonation of the newly built complex by the protonated phosphine (middle row), and oxidative deprotonation of the azole N–H group by the Ni^0 complex followed by substitution of a phosphine ligand in the newly built Ni^{II} complex by the azolato nitrogen atom (bottom row). Out of these three possibilities only the last one is energetically feasible under the reaction conditions since the activation barrier in the concerted oxidative addition reaction is 147.2 kJ/mol, and the deprotonated N-azolato complex appearing in the second algorithm is destabilized by 148.1 kJ/mol.

Reaction of [Ni(COD)(PMe$_3$)$_2$]/PMe$_3$ with 8-chlorotheophylline

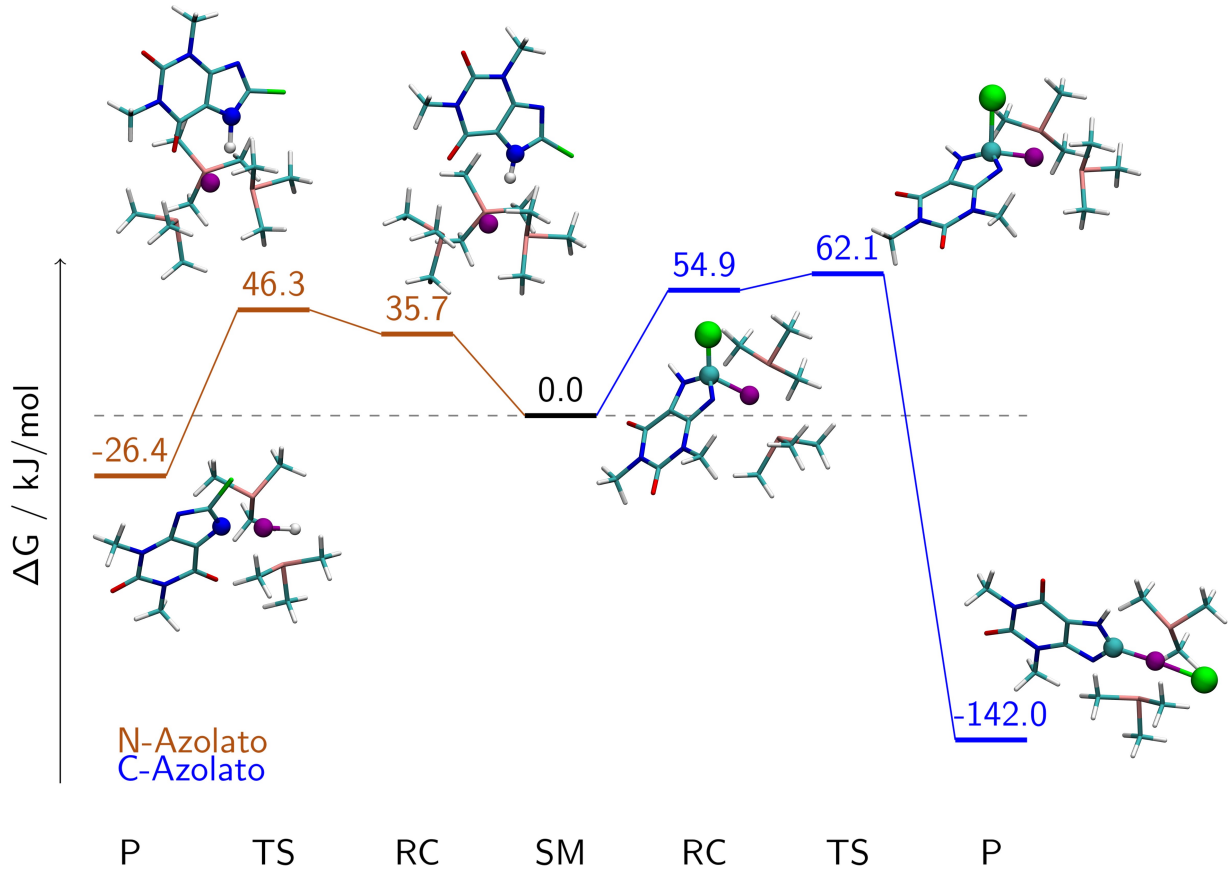

Figure S3. Reaction profiles towards the N-azolato (hydride) and the C-azolato (carbene) reaction products for the reaction of [Ni(COD)$_2$]/PMe$_3$ with 8-chlorotheophylline in the presence of an excess of phosphine ligand.

Figure S3 shows a comparison of the reaction profiles for the reaction of [Ni(COD)$_2$]/PMe$_3$ with 8-chlorotheophylline in presence of an excess of phosphine ligand towards the N-azolato (hydride) and C-azolato (carbene) products, respectively. The starting materials (SM) are defined as [Ni(COD)(PMe$_3$)$_2$] + PMe$_3$ + 8-chlorotheophylline. For the formation of the N-azolato reaction product, first a reaction complex (RC), comprised of a (now free) COD ligand, and a complex of 8-chlorotheophylline and Ni(PMe$_3$)$_3$, is formed that is destabilized by 35.7 kJ/mol. Small geometrical changes in the complex of 8-chlorotheophylline and Ni(PMe$_3$)$_3$ lead to the transition state (TS), which is 46.3 kJ/mol higher in

energy than the starting materials (SM). The reaction coordinate of this transition state describes a proton transfer from 8-chlorotheophylline to the metal center. Exchange of a PMe_3 ligand with the now deprotonated 8-chlorotheophylline yields the N-azolato product (P) that is 26.4 kJ/mol more stable than the starting materials.

In order to arrive at the C-azolato (carbene) product, a RC must be formed that is 54.9 kJ/mol less stable than the SM. This RC is comprised of an η^2-complex of 8-chlorotheophylline and $Ni(PMe_3)_2$, and a free PMe_3 ligand as well as a free COD ligand. Small geometrical changes in the complex of 8-chlorotheophylline and $Ni(PMe_3)_2$ yield the TS, which is 62.1 kJ/mol less stable than the starting materials. Here, the reaction coordinate describes a S_N^2-type oxidative addition, where the metal center substitutes the chloride anion. After coordination of the chloride anion to the metal center, the very stable product, stabilized by 142.0 kJ/mol, is formed. At temperatures sufficiently low to suppress the formation of the C-azolato product, the N-azolato product should be formed exclusively. If temperatures are high enough to surpass the higher activation barrier towards the C-azolato product, then this product should be formed in high yield due to its high thermodynamic stability.

Reaction of [Pd(COD)$_2$]/PMe$_3$ with 8-chlorotheophylline

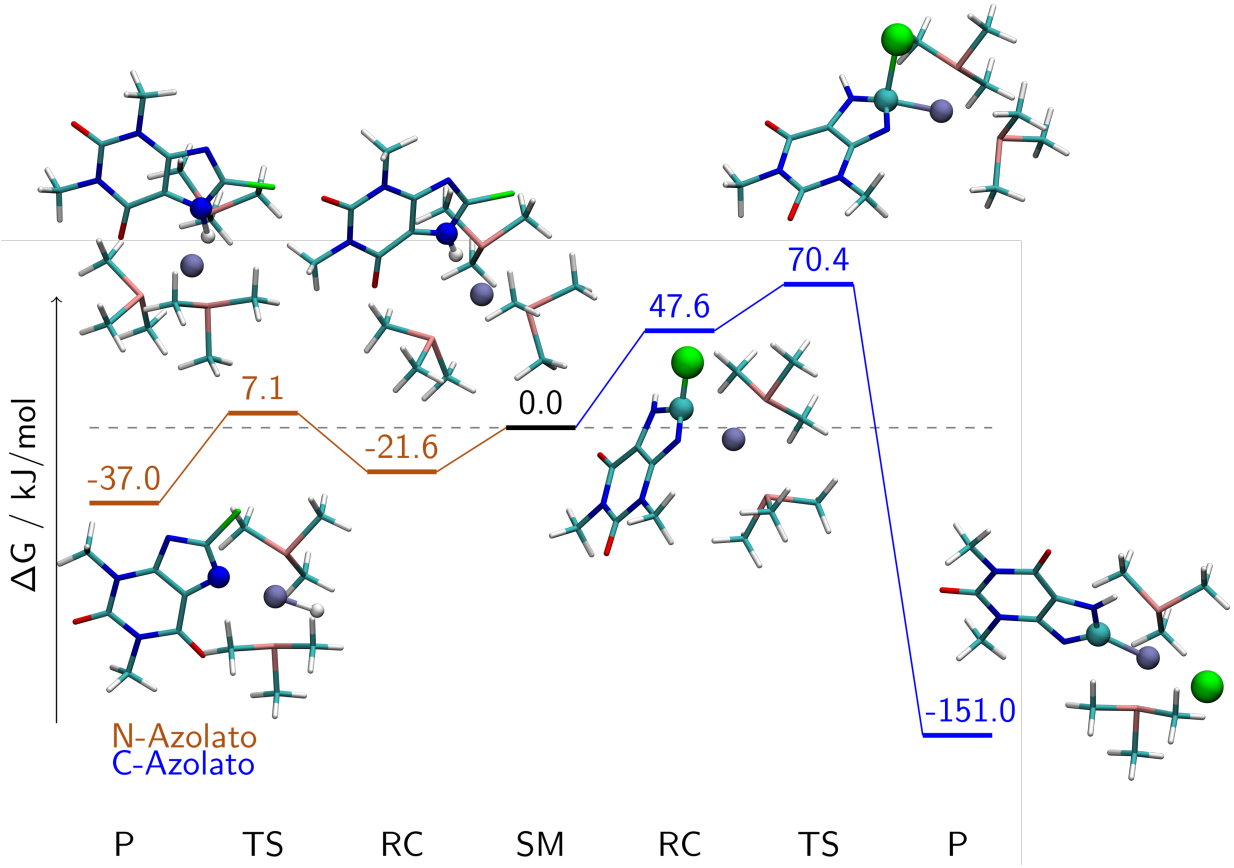

Figure S4. Reaction profiles towards the N-azolato (hydride) and the C-azolato (carbene) reaction products for the reaction of [Pd(COD)$_2$]/PMe$_3$ with 8-chlorotheophylline in presence of an excess of phophine ligand.

Figure S4 summarizes the reaction of [Pd(COD)$_2$]/PMe$_3$ in the presence of an excess of phosphine ligand with 8-chlorotheophylline. The starting materials, reaction complexes, transition states, and products are defined analogously to those in the reaction of [Ni(COD)$_2$]/PMe$_3$ with 8-chlorotheophylline. In order to obtain the N-azolato product, first a reaction complex is formed that is stabilized by 21.6 kJ/mol compared to the starting materials. A transition state is passed that is 7.1 kJ/mol less stable than the starting materials, resulting in a total activation barrier of 28.7 kJ/mol. The transition state again describes a proton transfer from 8-chlorotheophylline to the Pd complex. A subsequent ligand exchange leads the final product, stabilized by 37.0 kJ/mol.

The C-azolato product is obtained by forming a reaction complex that is destabilized by 47.6 kJ/mol. A transition state of 70.4 kJ/mol is passed, resulting in the thermodynamically most stable C-azolato product, stabilized by 151.0 kJ/mol.

Again, the N-azolato product is the kinetically controlled product, while the C-azolato product will be formed in a thermodynamically controlled reaction. Compared to the analogous reaction of $[Ni(COD)_2]/PMe_3$, the C-azolato pathway shows a very similar behavior, while the N-azolato pathway is much more favorable in the reaction of $[Pd(COD)(PMe_3)_2]$.

Reaction of [Pd(PPh$_3$)$_4$] with 8-chlorotheophylline

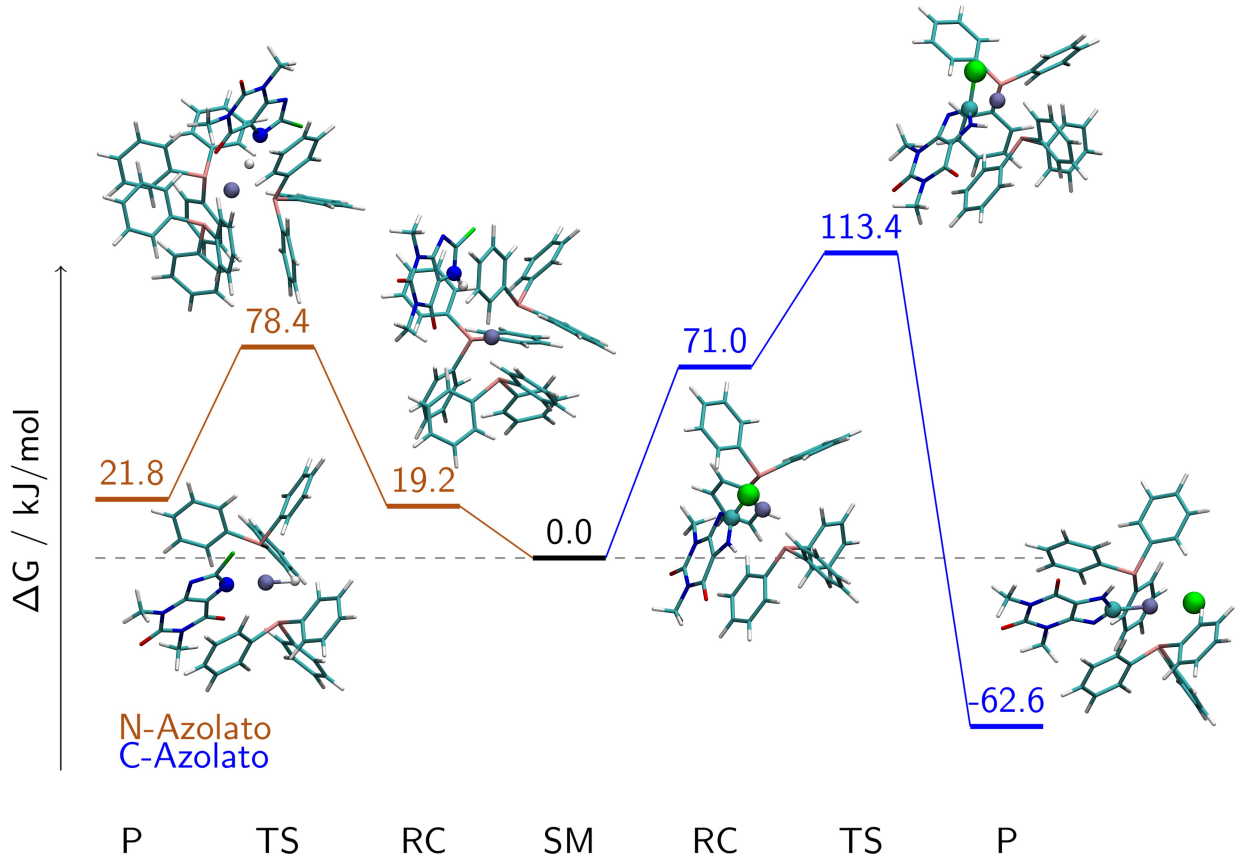

Figure S5. Reaction profiles towards the N-azolato (hydride) and the C-azolato (carbene) reaction products for the reaction of [Pd(PPh$_3$)$_4$] with 8-chlorotheophylline.

For the reaction of [Pd(PPh$_3$)$_4$] with 8-chlorotheophylline, the reaction profiles are summarized in Figure S5. Here, the starting materials are [Pd(PPh$_3$)$_4$] and 8-chlorotheophylline. The RC towards the N-azolato (hydride) product, defined as the complex of [Pd(PPh$_3$)$_3$] and 8-chlorotheophylline and a free PPh$_3$ ligand, is now only 19.2 kJ/mol less stable than the SM, followed by a TS, accessible through small geometrical changes in the RC, of 78.4 kJ/mol. Again, the reaction coordinate describes a proton transfer from 8-chlorotheophylline to the metal center. The final reaction product, comprised of the N-azolato product and two free PPh$_3$ ligands, is destabilized by 21.8 kJ/mol. Compared to the reaction of 8-chlorotheophylline with [Ni(COD)$_2$]/PMe$_3$ (Figure S3), the RC is now 16.5 kJ/mol more stable. The

TS for the N-azolato product, however, is 32.1 kJ/mol higher in energy than in the reaction with [Ni(COD)(PMe_3)$_2$]. Compared to the analogous reaction with [Pd(COD)$_2$]/PMe_3 (Figure S4), RC and TS are 40.8 kJ/mol and 71.3 kJ/mol higher in energy. This is likely to be a result of the higher basicity of the metal center in [Pd(COD)$_2$]/PMe_3 due to the presence of the more donating PMe_3 ligands (compared to the PPh_3 present in [Pd(PPh_3)$_4$]).

The reaction profile leading to the C-azolato (carbene) reaction product passes through an RC, containing an η^2-complex of 8-chlorotheophylline and [Pd(PPh_3)$_2$], and two free PPh_3 ligands, with an energy of 71.0 kJ/mol relative to the SM, followed by a TS of 113.4 kJ/mol. This TS again describes an S_N^2-type oxidative addition, where a chloride anion is substituted. The final reaction product is then formed by coordination of this chloride anion to the metal center and is stabilized by 62.6 kJ/mol. Comparing this to the reaction with [Ni(COD)$_2$]/PMe_3 the RC is again by 16.1 kJ/mol less stable. Furthermore, the TS is 51.3 kJ/mol higher in energy than the TS of the reaction of [Ni(COD)$_2$]/PMe_3 with 8-chlorotheophylline. Comparison with the reaction of [Pd(COD)$_2$]/PMe_3 with 8-chlorotheophylline shows a RC and TS that are 23.4 kJ/mol and 43.0 kJ/mol more destabilized, respectively.

From these results we conclude that the N-azolato (hydride) product might form at lower temperatures as a kinetically favored product. However, it will be in equilibrium with the starting materials. The C-azolato (carbene) product will be formed as the thermodynamically favored reaction product if temperatures are sufficiently high to overcome the large barrier of 113.4 kJ/mol, which also explains the high temperatures needed in the synthesis of the C-azolato reaction product.

Reaction of [Ni(COD)(PMe$_3$)$_2$]/PMe$_3$ with 2-chlorbenzimidazole

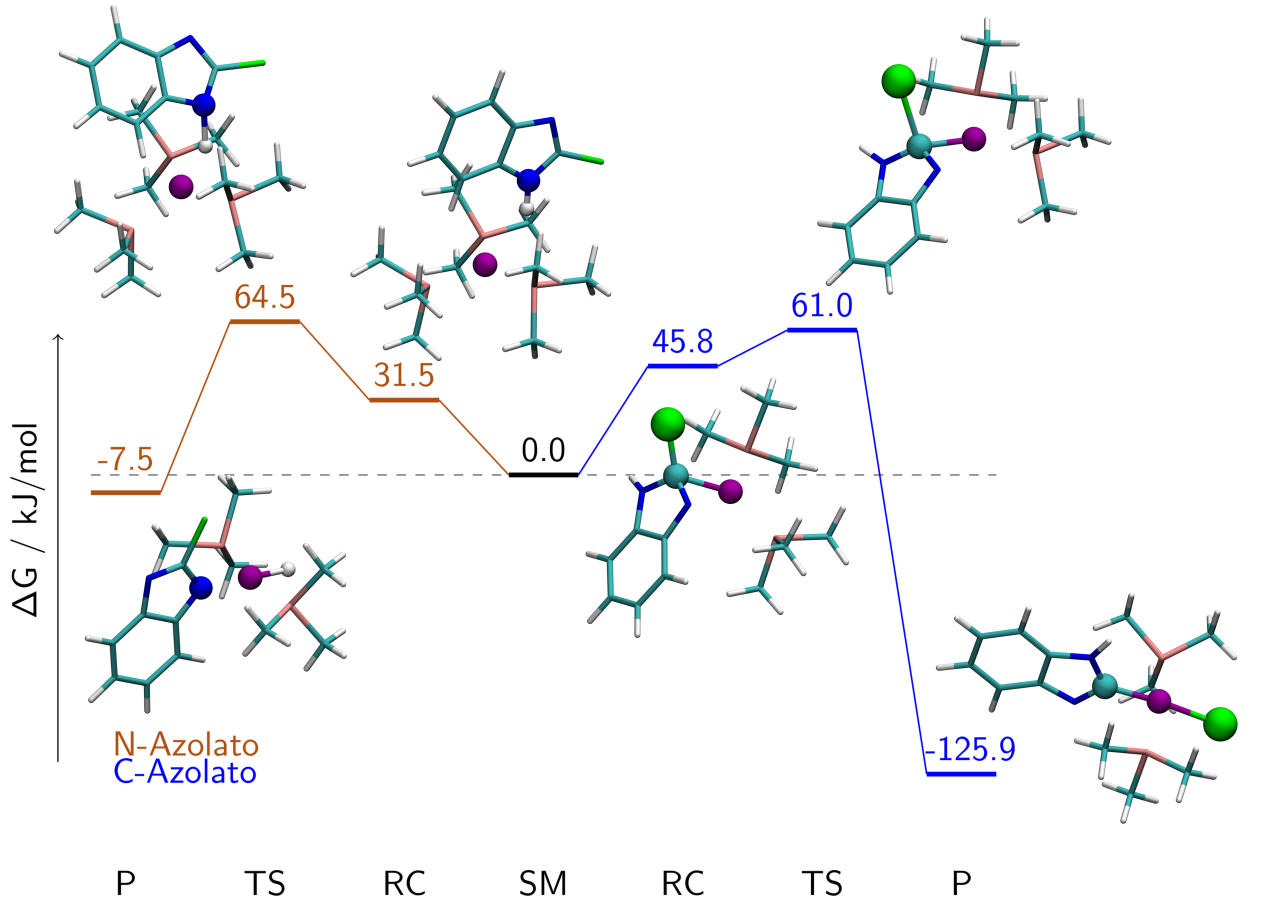

Figure S6. Reaction profiles towards the N-azolato (hydride) and the C-azolato (carbene) reactions products for the reaction of [Ni(COD)$_2$]/PMe$_3$ with 2-chlorobenzimidazole in the presence of an excess of phosphine ligand.

Figure S6 summarizes the reaction of [Ni(COD)$_2$]/PMe$_3$ in the presence of an excess of PMe$_3$ with 2-chlorobenzimidazole. The starting materials, reaction complexes, transition states, and products a defined analogously to those in the reaction of [Ni(COD)$_2$]/PM$_3$ with 8-chlorotheophylline. Although the experimental data for the reaction of [Ni(COD)$_2$]/PMe$_3$ with 2-chlorobenzimidazole supports the theoretical findings of a kinetically controlled N-azolato (hydride) product (at low temperature) and a thermodynamically favored C-azolato (carbene) reaction product (at elevated temperature), the computational results predict the C-azolato (carbene) reaction product to be kinetically and

thermodynamically favored (Figure S6). However, it should be noted that, in contrast to the other reactions studied here, the differences in the activation barriers for this specific example $\Delta\Delta G$ = 3.5 kJ/mol are too subtle to be resolved accurately using DFT methods and are within the typical error bar of the employed exchange-correlation functional for transition-metal systems.[12]

References

1. Hooft, R. W. W. Bruker AXS, **2008**, Delft, The Netherlands.
2. Otwinowski, Z.; Minor, W. *Methods Enzymol.* **1997**, *276*, 307.
3. Otwinowski, Z.; Borek, D.; Majewski, W.; Minor, W. *Acta Crystallogr*. **2003**, *A59*, 228.
4. Sheldrick, G. M. *Acta Crystallogr*. **1990**, *A46*, 467.
5. Sheldrick, G. M. *Acta Crystallogr*. **2008**, *A64*, 112.
6. TURBOMOLE V7.2 2017, a development of University of Karlsruhe and Forschungszentrum Karlsruhe GmbH, 1989-2007, TURBOMOLE GmbH, since 2007; available from http://www.turbomole.com.
7. Perdew, J. P.; Ernzerhof, M.; Burke, K. *J. Chem. Phys.* **1996**, *105*, 9982.
8. Grimme, S.; Antony, J.; Ehrlich, S.; Krieg, H. *J. Chem. Phys.* **2010**, *132*, 154104.
7. Grimme, S.; Ehrlich, S.; Goerigk, L. *J. Comp. Chem.* **2011**, *32*, 1456.
10. Steinmetz, M.; Grimme, S. *ChemistryOpen* **2013**, *2*, 115.
11. Andrae, D.; Häußermann, U.; Dolg, M.; Stoll, H.; Preuß, H. *Theoretica Chim. Acta* **1990**, *77*, 123.
12. Klamt, A. *J. Phys. Chem.* **1995**, *99*, 2224.

NMR Spectra of all new compounds (Figures S7–S24)

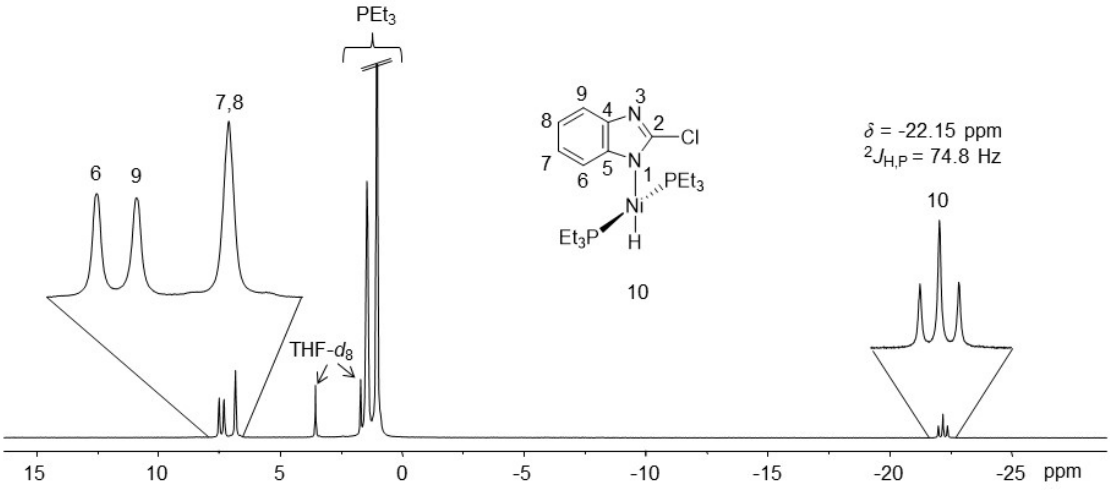

Figure S7. ^{1}H NMR spectrum of *trans*-[**4**] in THF-d_8.

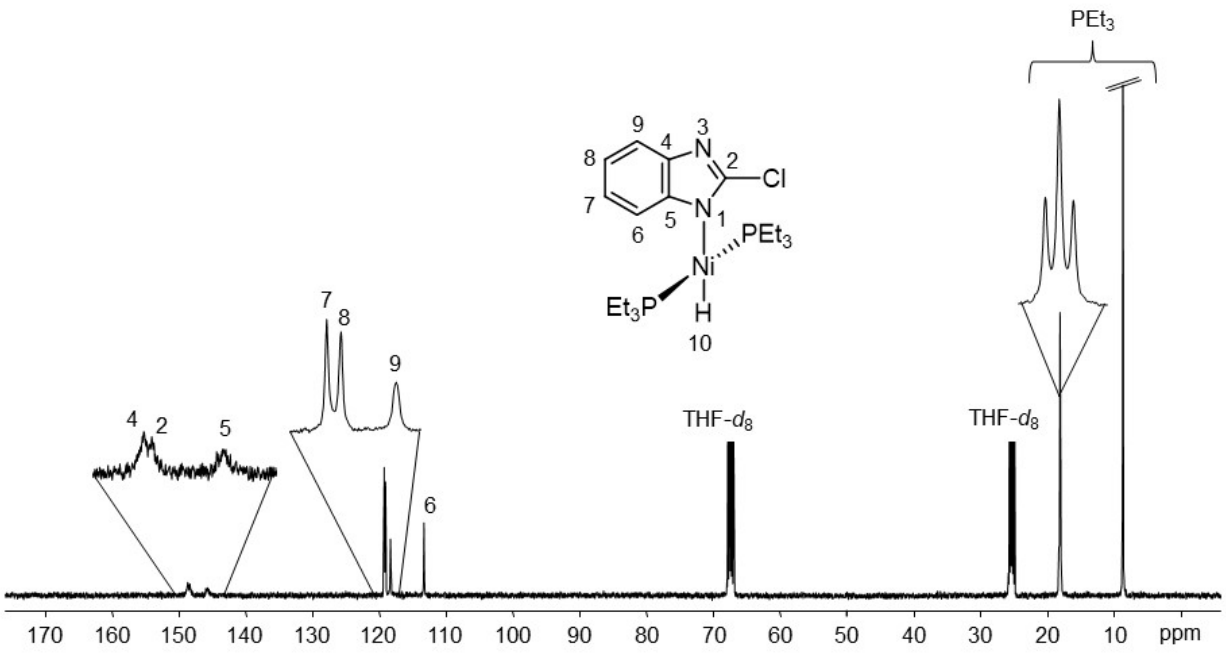

Figure S8. ^{13}C{^{1}H} NMR spectrum of *trans*-[**4**] in THF-d_8.

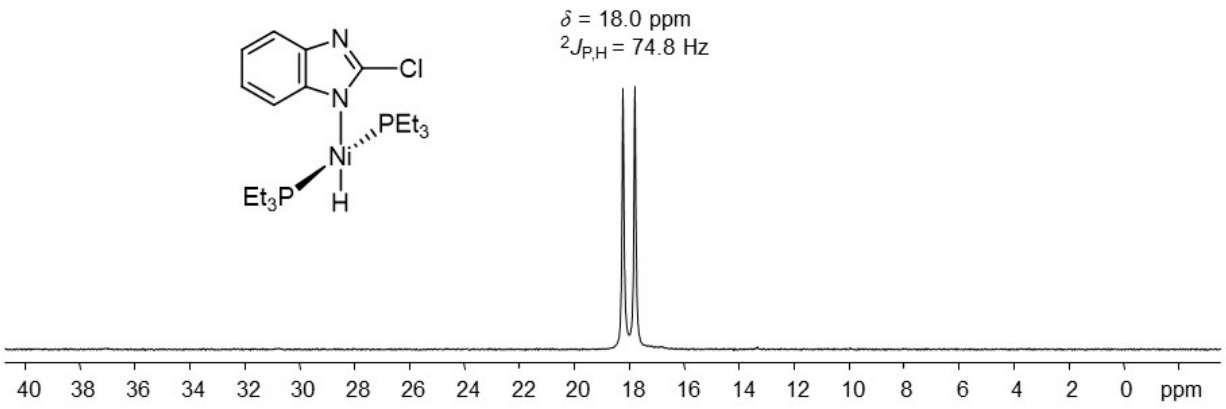

Figure S9. $^{31}P\{^1H\}$ NMR spectrum of *trans*-[**4**] in THF-d_8.

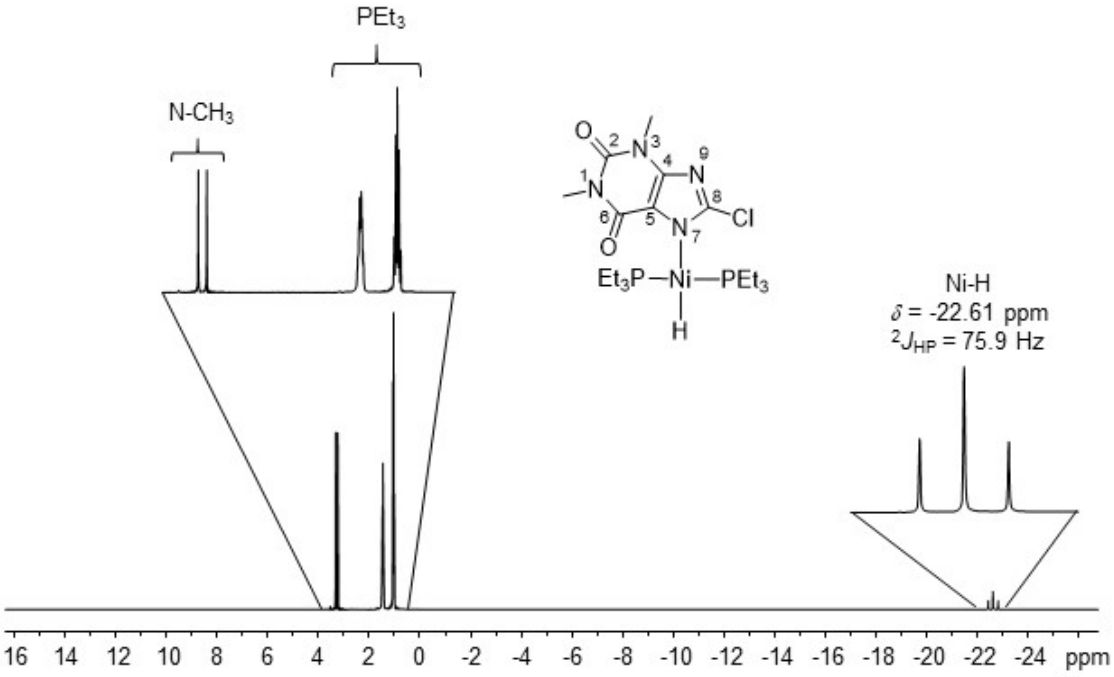

Figure S10. ^1H NMR spectrum of *trans*-[**5**] in THF-d_8.

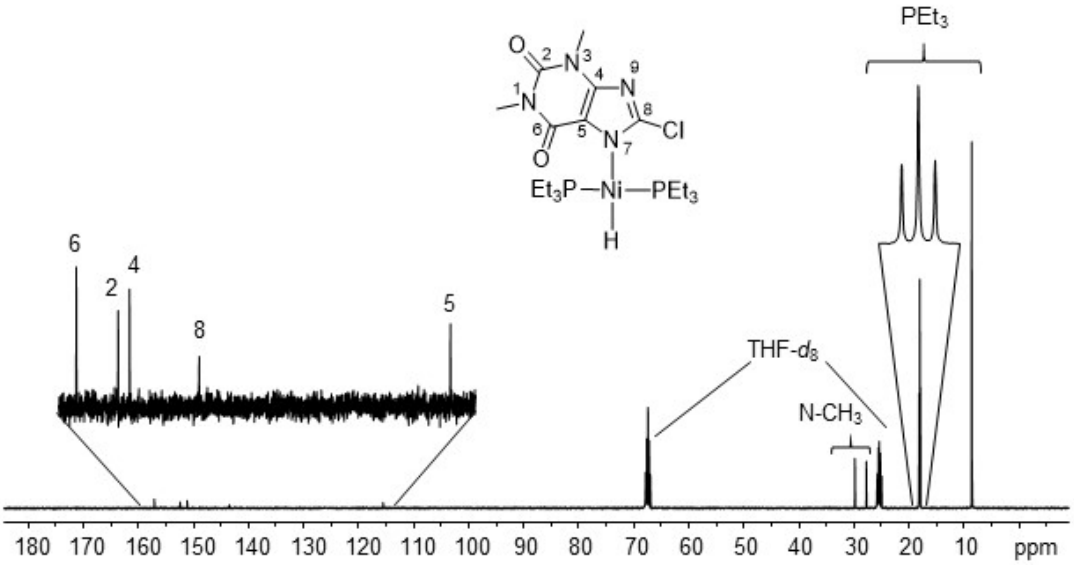

Figure S11. $^{13}C\{^{1}H\}$ NMR spectrum of *trans*-[**5**] in THF-d_8.

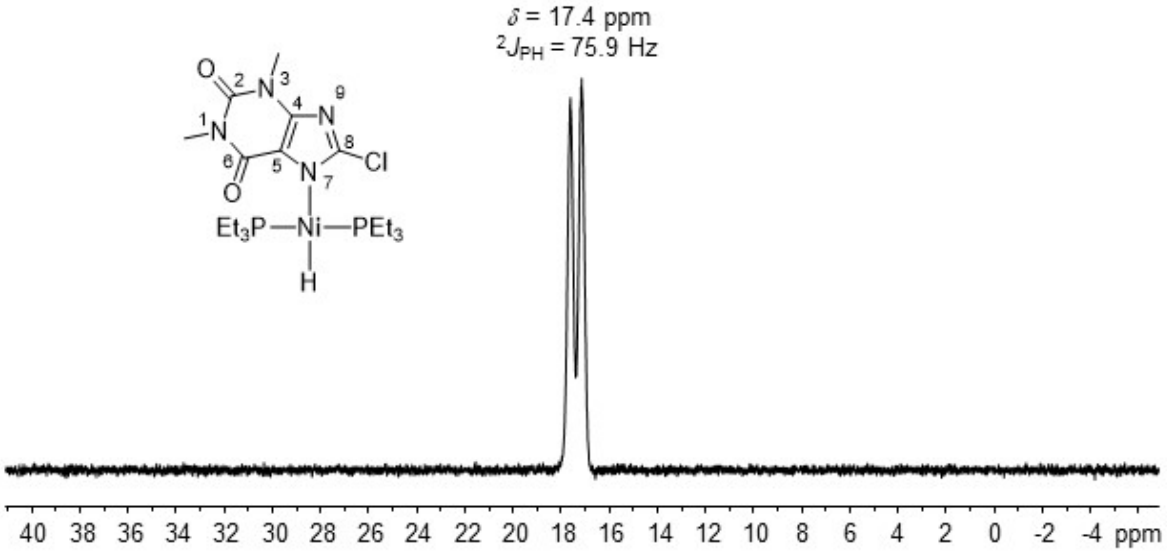

Figure S12. $^{31}P\{^{1}H\}$ NMR spectrum of *trans*-[**5**] in THF-d_8.

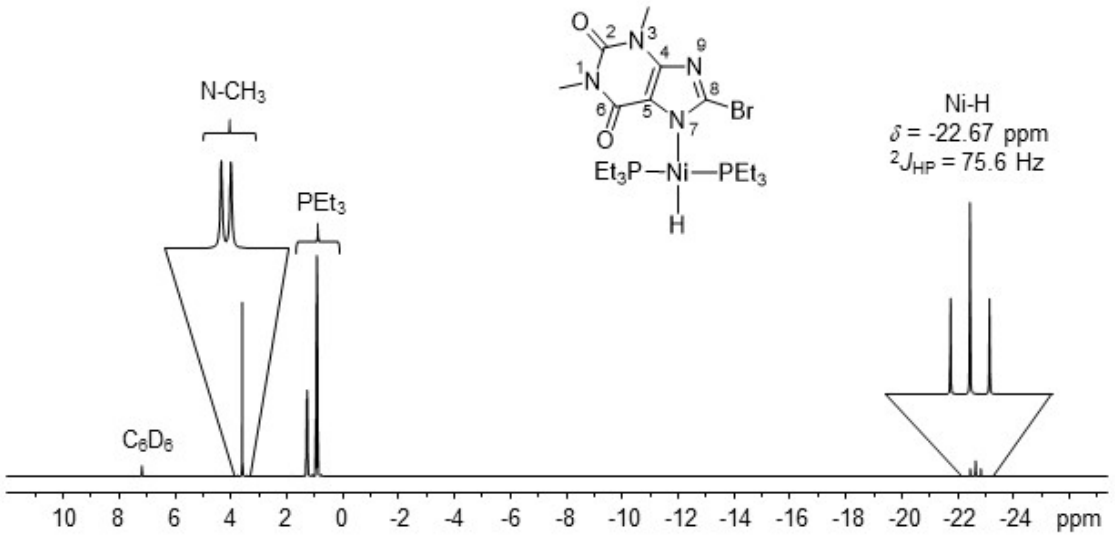

Figure S13. ^{1}H NMR spectrum of *trans*-[**6**] in C_6D_6.

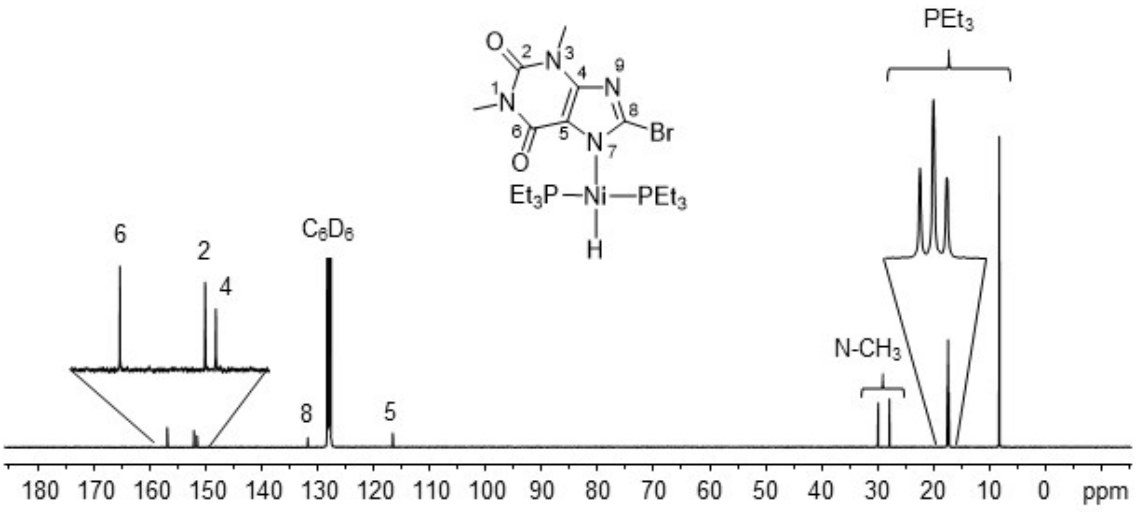

Figure S14. ^{13}C{^{1}H} NMR spectrum of *trans*-[**6**] in C_6D_6.

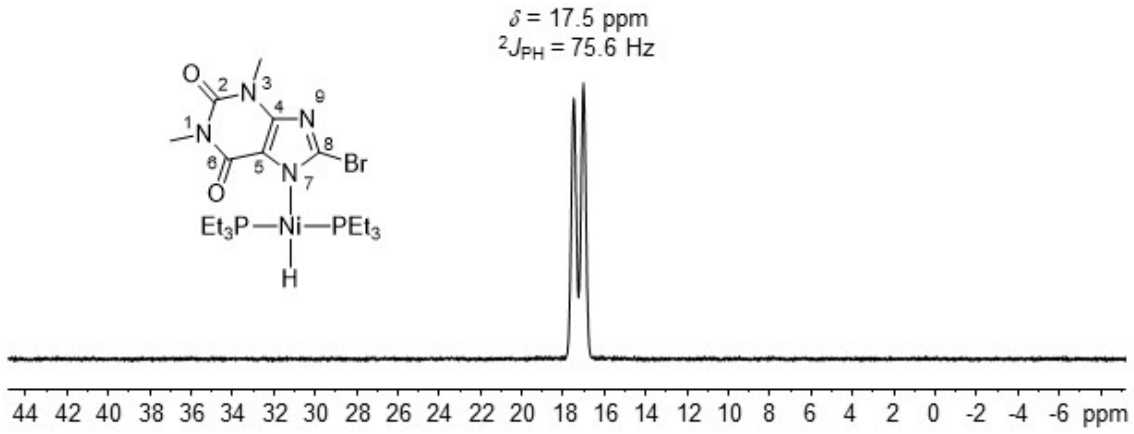

Figure S15. $^{31}P\{^1H\}$ NMR spectrum of *trans*-[**6**] in C_6D_6.

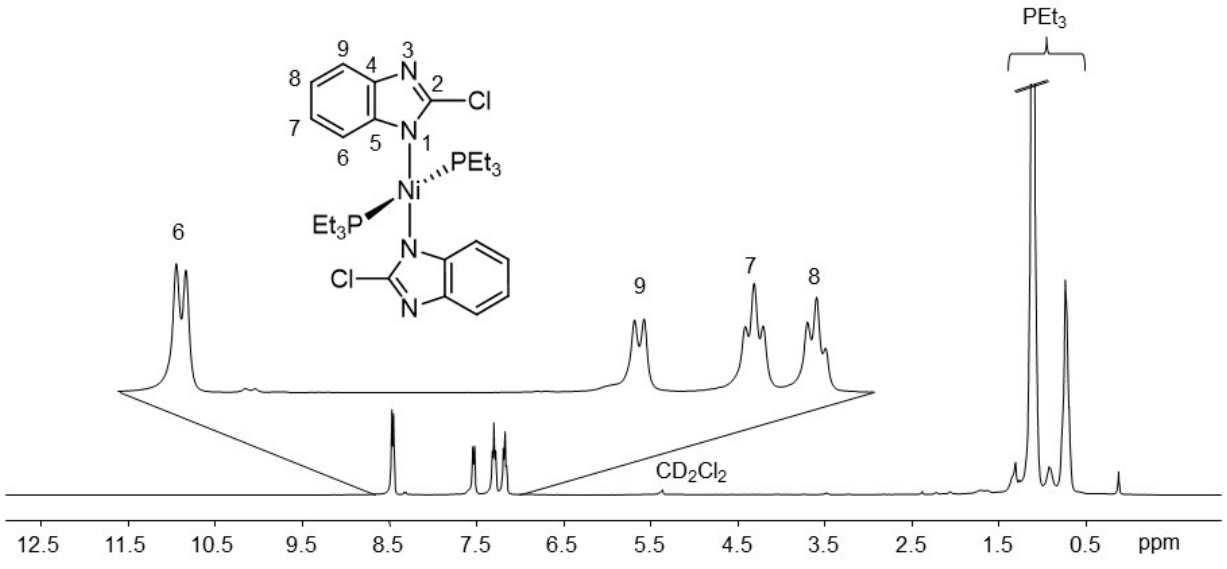

Figure S16. $\{^1H\}$ NMR spectrum of *trans*-[**7**] in CD_2Cl_2.

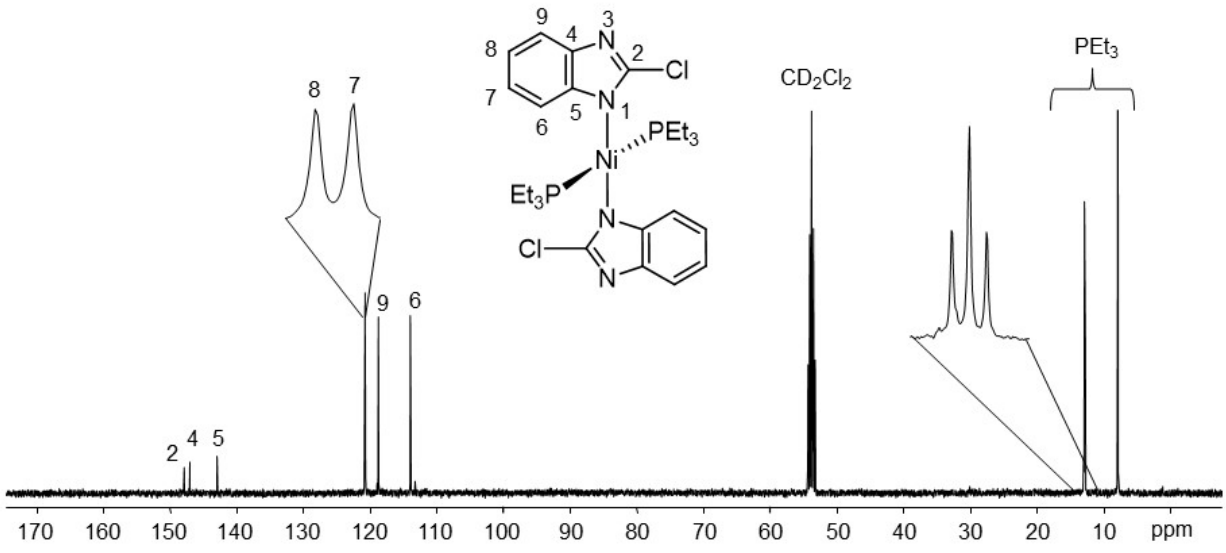

Figure S17. $^{13}C\{^{1}H\}$ NMR spectrum of *trans*-[**7**] in CD_2Cl_2.

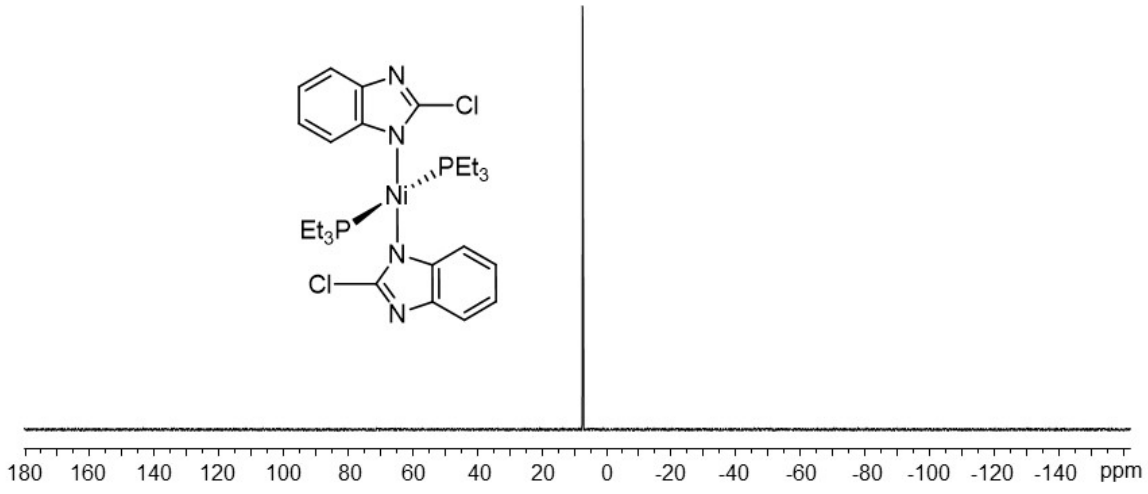

Figure S18. $^{31}P\{^{1}H\}$ NMR spectrum of *trans*-[**7**] in CD_2Cl_2.

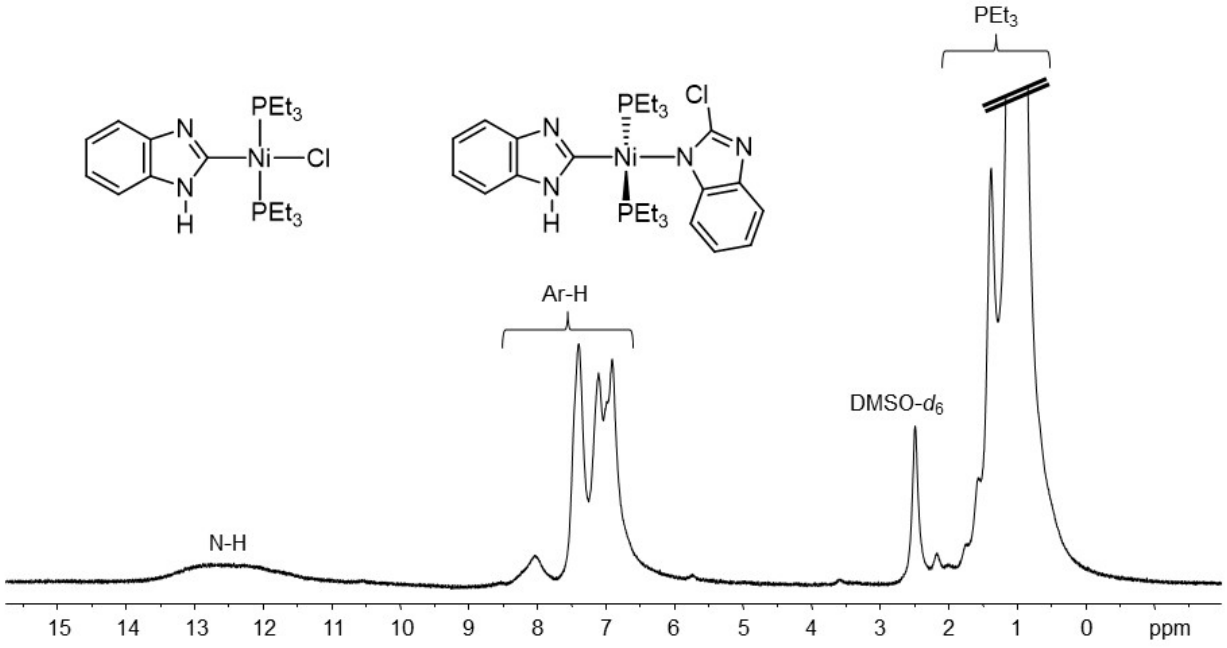

Figure S19. ^{1}H NMR spectrum of the *trans*-[**8**] and *trans*-[**9**] complex mixture in DMSO-d_6.

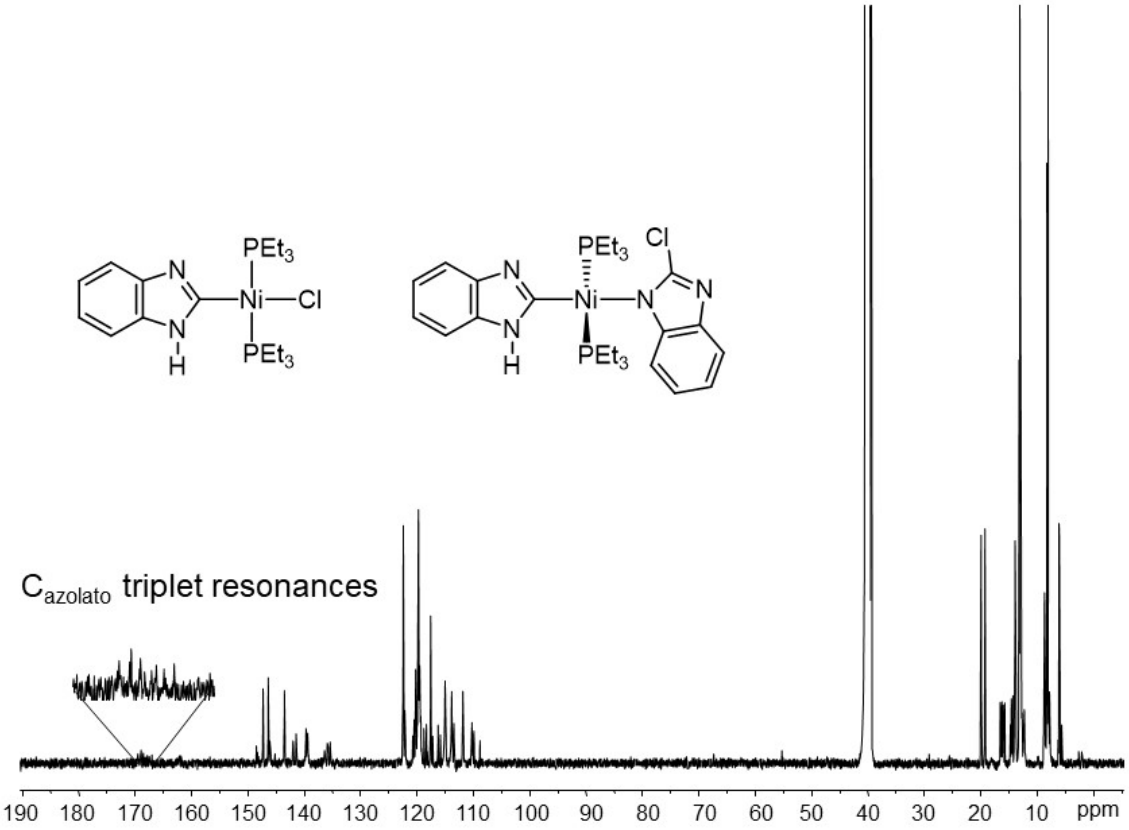

Figure S20. ^{13}C{^{1}H} NMR spectrum of the *trans*-[**8**] and *trans*-[**9**] complex mixture in DMSO-d_6.

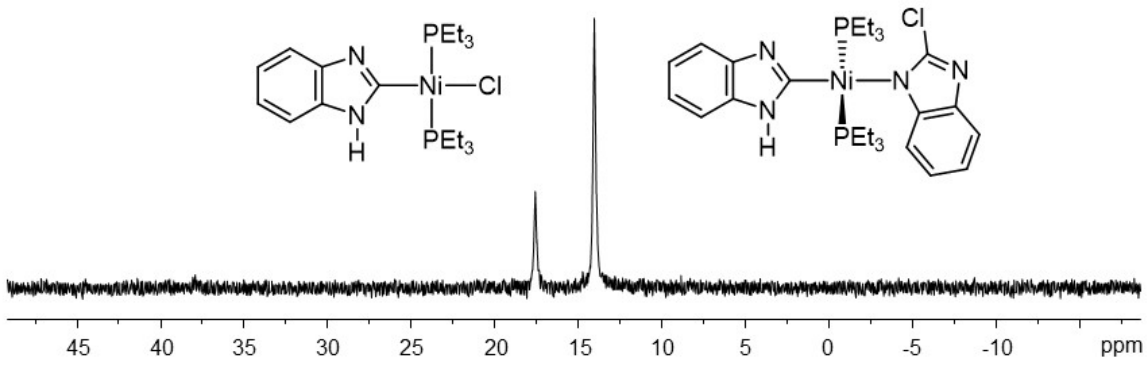

Figure S21. $^{31}P\{^{1}H\}$ NMR spectrum of the *trans*-[**8**] and *trans*-[**9**] complex mixture in DMSO-d_6.

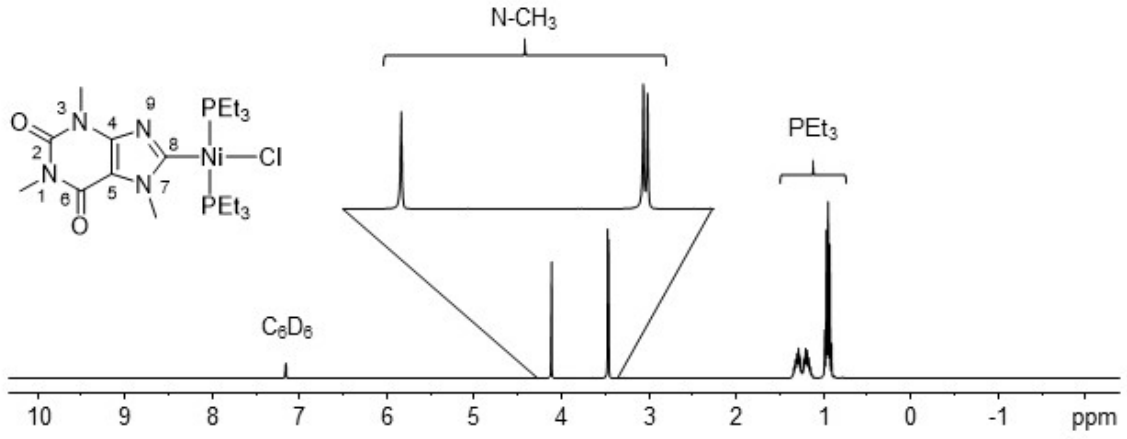

Figure S22. ^{1}H NMR spectrum of *trans*-[**10**] in C_6D_6.

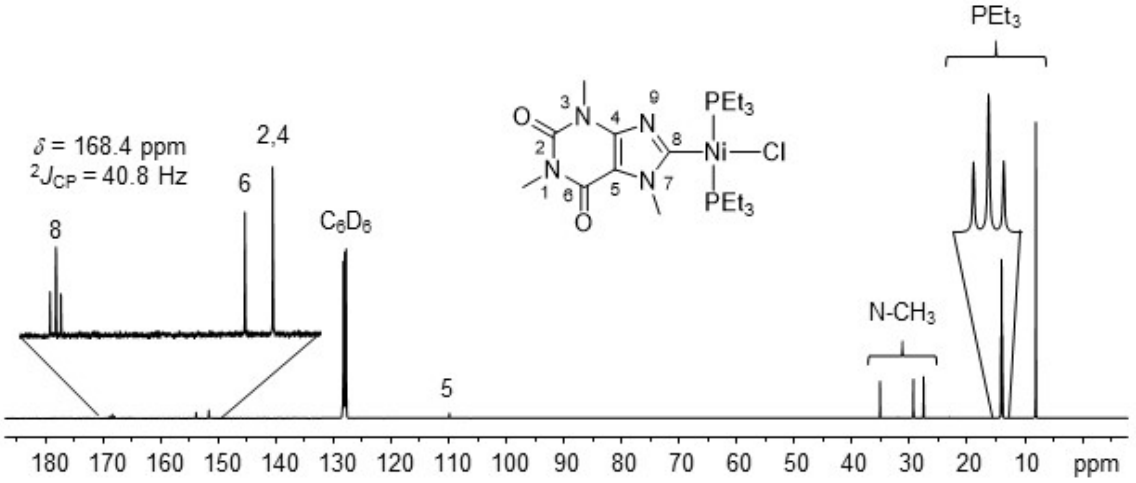

Figure S23. $^{13}C\{^{1}H\}$ NMR spectrum of *trans*-[**10**] in C_6D_6.

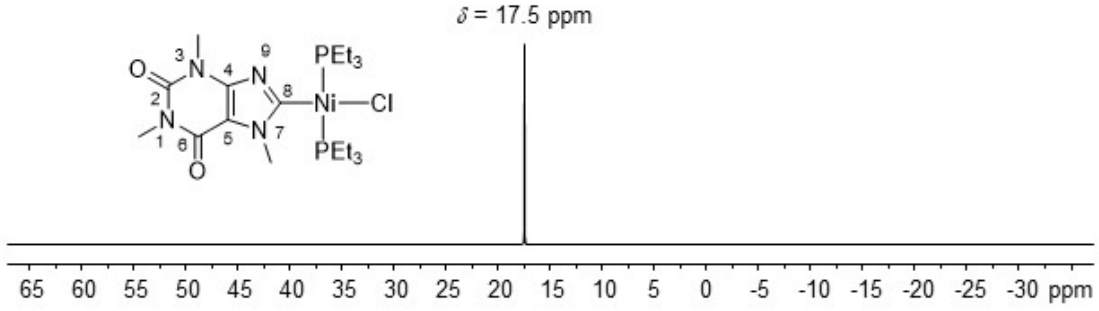

Figure S24. $^{31}P\{^{1}H\}$ NMR spectrum of *trans*-[**10**] in C_6D_6.